IEEE Photonics Journal
An IEEE Photonics Society Publication

Open Access

Transmission of 344 Gb/s 16-QAM Using a Simplified Coherent Receiver Based on Single-Ended Detection

Volume 8, Number 3, June 2016

Thang M. Hoang
Mohammed Y. S. Sowailem
Mohamed Morsy-Osman
Mathieu Chagnon
David Patel
Stéphane Paquet
Carl Paquet
Ian Woods
Odile Liboiron-Ladouceur
David Plant

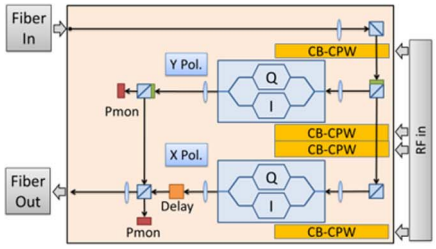

Thang M. Hoang et al.," Transmission of 344 Gb/s 16-QAM Using a Simplified Coherent Receiver Based on Single-Ended Detection," IEEE Photonics Technology Letters, vol. 8, issue. 3 pp., June1, 2016. DOI: 10.1109/JPHOT.2016.2574738

IEEE photonics SOCIETY

IEEE

Transmission of 344 Gb/s 16-QAM Using a Simplified Coherent Receiver Based on Single-Ended Detection

Thang M. Hoang,[1] Mohammed Y. S. Sowailem,[1] Mohamed Morsy-Osman,[1,2] Mathieu Chagnon,[1] David Patel,[1] Stéphane Paquet,[3,4] Carl Paquet,[3,4] Ian Woods,[3,4] Odile Liboiron-Ladouceur,[1] and David Plant[1]

[1]Department of Electrical and Computer Engineering, McGill University, Montreal, QC H3A 0E9, Canada
[2]Department of Electrical Engineering, Alexandria University, Alexandria 12544, Egypt
[3]TeraXion, Inc., Einstein, QC 2716, Canada
[4]Ciena Corporation, Einstein, QC 2716, Canada

DOI: 10.1109/JPHOT.2016.2574738

Manuscript received March 25, 2016; revised May 3, 2016; accepted May 27, 2016. Date of publication June 1, 2016; date of current version June 7, 2016. Corresponding author: T. M. Hoang (e-mail: thang.hoang@mail.mcgill.ca).

Abstract: We demonstrate a single-wavelength, 344-Gb/s, 43-Gb 16-quadrature amplitude modulation (QAM) polarization division multiplexed signal transmission over 800 km operating below the hard-decision forward error correction (FEC) BER threshold of 3.8×10^{-3} using an InP dual-polarization in-phase/quadrature modulator. At the receiver, a simplified single-ended coherent receiver with novel digital signal processing (DSP) for self-beating noise removal is employed. Compared with the conventional single-ended detection, this signal processing method doubles the propagation distance and increases the SNR by more than 1 dB. In addition, this DSP method provides 10 dB of the received optical power dynamic range while operating below the hard-FEC BER threshold of 3.8×10^{-3}, compared with the no dynamic range for a single-ended receiver without the proposed DSP.

Index Terms: Coherent receiver, in-phase/quadrature (I/Q) modulator, single-ended detection (SED).

1. Introduction

The need for higher capacities in short reach and metro optical communication links has created demand for systems operating at unprecedented bit rates. This goal can be achieved by using several approaches, one of which is to use high baud rates with relatively lower modulation efficiency, as demonstrated in [1]. In [1], a super-Nyquist filter was used to reduce the signal bandwidth of a 110 Gbaud polarization-division-multiplexed quadrature phase shift keying (PDM-QPSK) signal to fit 100 GHz grid. Another alternative is to use a high spectral efficiency modulation format such as high order quadrature amplitude modulation (M-QAM) [2]–[4]. At such high baud rate experiments, digital-signal-processing (DSP) at the transmitter and receiver is necessary to mitigate the impairments of the transceiver and optical link. Additional increases in speed can be obtained via multiplexing either in wavelength, e.g., dual-carrier 32 Gbaud PDM-16-QAM [5], or in time [6]. For an equal bit rate, modulating a single carrier from a single laser provides a solution that is cost

effective relative to a hardware multiplexed alternative which involves the use of multiple wavelengths or fiber lanes to achieve the same total desired capacity.

However, obtaining higher data rates with lower transmitter complexity, including package size, and power dissipation is challenging. Indium phosphide(InP) Mach–Zehnder modulators (MZM) have both high bandwidths and low operating voltages, with published values of V_π ranging from 1 to 2.5 V and bandwidths from 12 to 36 GHz[7]–[9]. In addition, InP devices can be integrated with other electrical or optical components such as lasers, RF amplifiers and optical amplifiers [7], [9], [10]. All of these features enable the reduction of both package size and power consumption. Several single wavelength transmissions have been demonstrated using InP IQ modulators, with different reported values of distances, data rates, and modulation formats. Among those experiments, 32 Gbaud PM-QPSK and PM-16-QAM transmission over 8000 km, and 960 km, respectively, was demonstrated at the soft decision forward error correction (SD-FEC) threshold of 2×10^{-2} [7]. In addition, in [11] transmission of 28 Gbaud 64-QAM modulated signal over 40 km at a BER of 10^{-2} is shown.

The above systems all utilize balanced-detection (BD) based coherent receivers. To recover the transmitted signals, coherent receivers linearly map the in-phase (I) and quadrature (Q) components of the received optical signal to the electrical domain by mixing the received optical field with that of a local oscillator (LO). This direct mapping enables digital signal processing, which then allows the use of spectrally efficient modulation formats and also transmission impairment mitigation [12]. There are two main approaches, with their respective tradeoffs, to implement coherent receivers reception: i) balanced detection (BD), which is commonly used in commercialized integrated coherent receivers (ICR); and ii) single-ended detection (SED) [13], [14], [17]–[19]. BD ICRs have a high common-mode rejection ratio which reduces self-beating noise and make them suitable for high fidelity applications (e.g, long-haul transmission). Alternatively, SED ICRs can be realized with a simpler front-end and are thus more compact and less expensive. They can be applied when a larger penalty for both Q-factor and dynamic range is acceptable [13], [15], [16]. Since a compact transceiver form factor is a desirable feature for metro application [20], SED ICR research is of immense interest to reduce receiver complexity.

In this paper, we successfully demonstrate 344 Gbps transmission (300 Gbps payload) below the hard decision forward error correction (HD-FEC) threshold of 3.8×10^{-3} over 800 km of standard single mode fiber using an InP dual polarization IQ modulator (DP-IQM) and SED ICR implementation. Specifically, the system uses a 2.5 V_π InP DP-IQM on a single carrier operating at symbol rate of 43 Gbaud 16-QAM and a SED ICR with DSP incorporating an additional function that removes unwanted self-beating noise. The proposed algorithm allows for an additional 300 km of propagation and improves the SNR relative to conventional SED receiver by more than 1 dB. In addition, this DSP method provides 10 dB of received optical power dynamic range while operating below the HD-FEC BER threshold of 3.8×10^{-3}.

2. Experimental Setup and DSP Procedure

2.1. Experimental Setup

Fig. 1 presents the setup used for transmission experiments using the InP-based DP-IQM with DP-16QAM modulation. We used the same experimental setup as well as parts of DSP blocks to demonstrate the feasibility of utilizing DP-IQM for high data rate experiment [21]. The DP-IQM used in this experiment is packaged in a 41 mm by 19 mm module and uses two InP chip on carriers, as described in [8]. Fig. 2 shows a schematic illustrating the DP-IQM layout. The extinction ratios at 1550 nm (in dB) of the child MZMs are 29.91 and 30.91 for the *X* polarization modulator and 29.68 and 43.88 for the *Y* polarization modulator. Over the entire *C*-band, the worst case extinction ratio is 25 dB and the largest insertion loss of the modulator is 10 dB. The V_π for this design is 2.5 V and the 3-dB bandwidth is greater than 35 GHz for all MZM structures. An external cavity laser (ECL) at 1550.12 nm, with a linewidth of 100 kHz, and 15.5 dBm output power is used as the laser source. The four RF signal streams driving the InP-based DP-IQM are generated using a digital-to-analog

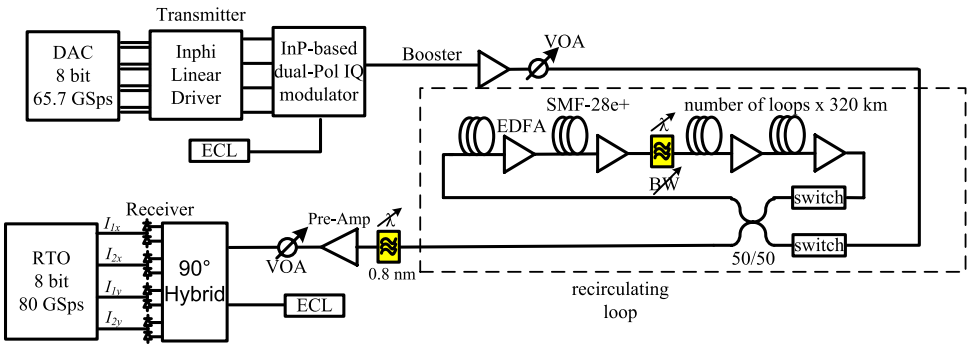

Fig. 1. Experimental setup.

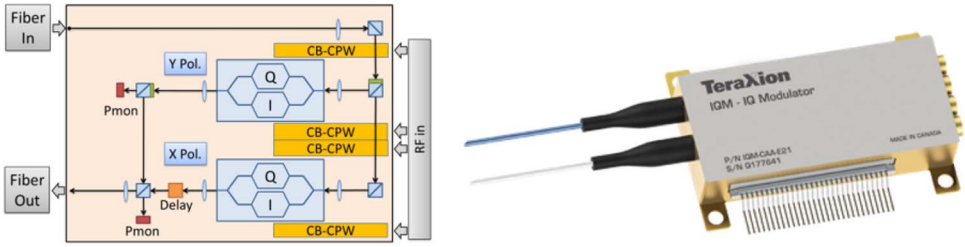

Fig. 2. InP DP-IQM (left) schematic and (right) module.

converter (DAC). The AC-coupled 8-bit DAC, running at 65.7 GSps, has four differential channels with a maximum output voltage of 1.2 V_{pp}. The differential outputs from the DAC channels are amplified by the RF linear driver to obtain four 5 V_{pp} RF single-ended signals to drive the InP DP-IQM. Afterwards, the optical signal is amplified to 23 dBm with a booster amplifier. The booster is followed by a variable optical attenuator (VOA) to adjust the signal power launched into the fiber to 1 dBm, which was empirically found to be the optimum launch optical power. The signal is then fed into an optical re-circulating loop controlled by switches. Each span in the loop has 80 km of SMF-28e+ fiber, followed by an inline erbium-doped fiber amplifier (EDFA) with a noise figure of 5 dB. The second span is followed by a 2-nm bandwidth tunable filter centered at a wavelength of 1550. 12 nm. The output signal from the re-circulating loop is connected to a 0.8 nm filter and is then pre-amplified to 9 dBm. Then, the pre-amplified signal is attenuated using a VOA to sweep the received power prior to the coherent receiver. A free-space-optics-based 90° optical hybrid is used to mix the received signal with a continuous wave (CW) light from another ECL laser with similar specifications to the one used at the transmitter. The optical hybrid is followed by balanced detection to eliminate the direct detection terms for referencing performance. To switch from the balanced detection to SED configuration, we disconnected the input to negative bias of the BD photodetector. After the coherent detection, the four signals are sampled by a 33 GHz 3 dB bandwidth real-time oscilloscope (RTO) running at 80 GS/s for offline DSP and serving as an 8-bit analog-to-digital (ADC).

2.2. DSP Procedure

As the system employs both DACs and ADCs, DSP can be applied at both the transmitter and the receiver. This section describes the different DSP schemes applied at both ends of the transmission system, from signal generation to signal detection, in order to best generate and recover the desired waveforms.

Fig. 3 illustrates the DSP process used in the transceiver. The transmitter DSP (Tx-DSP) starts with generating two independent streams of 16-QAM symbols uniformly distributed over four levels for dual polarization IQ transmission. The maximum number of symbols allowed by the

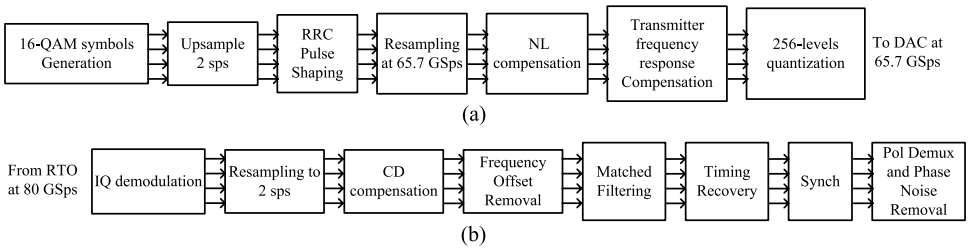

Fig. 3. DSP stacks at the (a) transmitter and (b) receiver side.

DAC were generated. Considering our oversampling factor (DAC sampling rate/baud rate) and the granularity of the DAC's memory, this turned out to be 165120 symbols. Because the maximum number of symbols allowed were chosen to fill the DAC's memory, the impact of the pattern length on the performance parameters such as BER and SNR was not investigated experimentally. After up-sampling the signal from one sample per symbol (sps) to two sps, a pulse shaping filter is applied using a root-raised-cosine (RRC) pulse with a roll-off factor of 0.4. Afterwards, the signals are re-sampled to the operating rate of the DAC at 65.7 GSps. This is followed by non-linear compensation for the inherent nonlinear MZM transfer function to keep the constellation points equally spaced after electrical-to-optical conversion. Next, the frequency response of the transmitter components (including i) the DAC, ii) the RF linear driver, and iii) the DP-IQM) is compensated using an FIR filter for digital pre-emphasis. The FIR filter was experimentally optimized at 43 Gbaud and had 61 effective taps. Finally, the RF pre-emphasis is followed by an 8-bit quantization process.

At the receiver, the DSP starts with IQ demodulation using the novel DSP for a SED based ICR. The details of the proposed DSP are described in the next section. After demodulation, the signal is resampled to two sps and then passed through typical DSP blocks: i) frequency domain chromatic dispersion (CD) compensation, ii) laser frequency offset compensation based on the Fast Fourier Transform of the signal at the 4th power, iii) matched filtering, iv) timing recovery, v) synchronization, and vi) polarization de-multiplexing and phase noise mitigation using training-symbol least mean square (TS-LMS) algorithm for initial convergence and decision-directed LMS (DD-LMS) for steady-state operation. After polarization de-multiplexing, the SNR calculation is done by measuring the noise power with transmitted symbols and subtracting that noise power from the total received signal power. The BER is directly counted over 900000 bits.

2.3. Proposed DSP for IQ Demodulation Using Single-Ended Detection

The derivation begins by modeling the photocurrent of any two outputs of an optical hybrid as

$$\begin{aligned} I_1 &= I_S + I_{LO} + 2\sqrt{I_S\ I_{LO}}\cos\varphi \\ I_2 &= I_S + I_{LO} + 2\sqrt{I_S\ I_{LO}}\cos(\varphi - \delta) \\ &= I_S + I_{LO} + 2\sqrt{I_S\ I_{LO}}[\cos\varphi\ \cos\delta + \sin\varphi\ \sin\delta] \end{aligned} \tag{1}$$

where I_S and I_{LO} are the photocurrents from the signal (S) and the LO, respectively; φ is the phase difference between the signal and the LO field; and δ is the optical phase shift of either the signal or the LO introduced in the second branch by the optical hybrid. In conventional AC coupled SED, the I_{LO} and the DC component of I_S are removed. However, the AC component of I_S still remains and degrades the fidelity of retrieved signal. Mathematically, (1) is a system of two independent equations with two unknowns φ and I_S. For the problem at hand, we propose an algorithm, based on the phase-shifting interferometry concept, to remove the self-beating noise $\alpha = I_S + I_{LO}$ [22]–[25]. The self-beating noise can be removed and I/Q components can be found from the following steps (the derivation is shown in the Appendix):

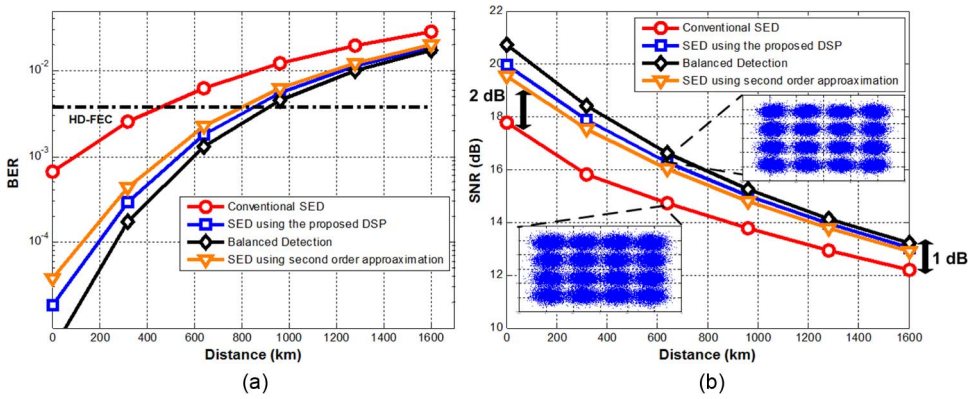

Fig. 4. Performance at received signal power of 2 dBm and LO power of 15.5 dBm. (a) Measured BER versus transmission distance. (b) (Inset) Measured SNR versus transmission distance and their constellations at 640-km transmission.

Step 1 Calculating α:

$$\alpha = \frac{-v - \sqrt{(v^2 - 4u\ w)}}{2u} \tag{2}$$

where

$$\begin{aligned} u &= 2(1 - \cos\delta) \\ v &= -2(1 - \cos\delta)(I_1 + I_2) - 4I_{\mathrm{LO}}\sin^2\delta \\ w &= (I_1 - I_2\cos\delta)^2 + I_2^2\sin^2\delta + 4I_{\mathrm{LO}}^2\sin^2\delta. \end{aligned} \tag{3}$$

Step 2 Calculating I/Q from α: For instance, in the case of a 2 $\times$ 2 SED with a 90° hybrid ($\delta = \pi/2$)

$$\begin{aligned} I_{I_{\mathrm{SED}}} &= I_1 - \alpha = 2\sqrt{I_S I_{\mathrm{LO}}}\cos\varphi \\ I_{Q_{\mathrm{SED}}} &= I_2 - \alpha = 2\sqrt{I_S I_{\mathrm{LO}}}\sin\varphi. \end{aligned} \tag{4}$$

The benefits of using the proposed algorithm with respect to conventional SED are twofold:

- The self-beating noise $\alpha = I_S + I_{\mathrm{LO}}$ is removed at the expense of additional DSP complexity. The complexity of the proposed DSP is only 13 N real operations (eight real adders and five real multipliers), where N is the number of processed samples per symbol for a 90° hybrid ($N = 2$ in this case). The complexity of a previously proposed algorithm using a second order approximation is 16 N real operations (eight real adders and eight real multipliers) [17].
- The phase-shift δ between the two optical branches of the hybrid can be any value in the range $0 < \delta < \pi$, thus relaxing the fabrication accuracy of the optical hybrid.

3. Results and Discussion

Fig. 4 shows the BER and the SNR versus the transmitted distance for a 43 Gbaud 16-QAM signal using four detection schemes: BD, conventional SED, SED using the presented DSP and SED using second order approximation DSP [17]. The LO power was set to 15.5 dBm and the received signal power was 2 dBm. In Fig. 4(a), SED with the proposed DSP (curve shown using blue squares) outperforms the conventional SED (curve shown using red circles) and slightly outperforms the receiver using second order approximation (curve shown using orange triangles) [17]. This BER versus distance curve tends to converge towards the BD curve (shown as

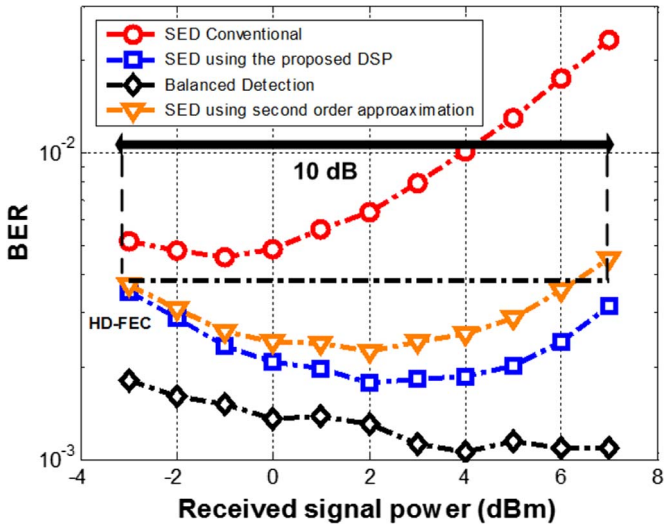

Fig. 5. Measured BER versus received signal power after 640-km transmission and an LO power of 15.5 dBm.

black diamonds) at longer distances. Although it is observed that a 344 Gbps signal can be transmitted over 400 km operating below the HD-FEC threshold using conventional SED, using the proposed DSP, the reach doubles and extends to 800 km.

In Fig. 4(b), we show the effectiveness of the proposed DSP in terms of SNR improvement of the SED approach. Relative to conventional SED, the SED with this proposed DSP gains 2 dB of SNR in the back-to-back configuration and approximately 1 dB of SNR at 800 km. The performance of SED using proposed DSP is comparable with that of SED using second order approximation in terms of SNR. Moreover, it is experimentally shown, for the first time, that the back-to-back SNR of both SED using the proposed DSP and second order approximation is only 1 dB below the SNR from balanced detection.

Fig. 5 shows the BER versus received signal power at the hybrid for a distance of 640 km and LO power of 15.5 dBm. With the received signal power varying from –3 to 7 dBm, the lowest achievable BER using the conventional SED is only 4.55×10^{-3} and is above the HD-FEC. However using our proposed DSP, the algorithm enables operation below the HD-FEC as well as a dynamic range of 10 dB, from –3 to 7 dBm of received signal optical power. At a received signal power of 2 dBm, the proposed algorithm improves the BER of SED from 6.4×10^{-3} down to 1.8×10^{-3}. The BER of the BD at this same signal power is 1.3×10^{-3}. Note that the performance of SED (both conventional and our proposed one) degrades at high received signal powers since the contribution of the remaining self-beating noise becomes significant in that regime. While the proposed SED has narrower dynamic range compared to BD, its BER is only marginally higher.

4. Conclusion

We experimentally demonstrated single wavelength, dual polarization, 43-Gbaud, 16 QAM transmission (344 Gbps) over 800 km of SMF below HD-FEC threshold of 3.8×10^{-3} using an InP dual-polarization IQ modulator and a SED coherent receiver, which employ a novel DSP algorithm to eliminate the distortion caused by self-beating noise in a SED ICR. This signal processing algorithm also allow to achieve 10 dB of dynamic range at 640 km and obtained an improvement of 1 dB in SNR compared to a conventional SED ICR. The use of the novel DSP algorithm presented in this paper is highly favorable, if a SED ICR is used at the receiver in a single carrier high-speed signal transmission for compact transceiver implementation along with a compact InP modulator for the transmitter.

Appendix

This Appendix shows the derivation of the closed-form solution of I/Q detection using phase-shifting interferometry concept. With reference to (1), we can re-organize the equations as

$$\begin{aligned}\sqrt{I_S}\cos\varphi &= \frac{I_1-\alpha}{2\sqrt{I_{LO}}}\\ \sqrt{I_S}\sin\varphi &= \frac{I_2-I_1\cos\delta-(1-\cos\delta)\alpha}{2\sqrt{I_{LO}}\sin\delta}.\end{aligned}\tag{5}$$

After taking the square of both sides of (5) and then taking their sum, we arrive at

$$\begin{aligned}(I_1-\alpha)^2\sin^2\delta+[I_2-I_1\cos\delta-(1-\cos\delta)\alpha]^2 &= 4I_{LO}I_S\sin^2\delta\\ &= 4I_{LO}(\alpha-I_{LO})\sin^2\delta\end{aligned}$$

or

$$\begin{aligned}2(1-\cos\delta)\alpha^2-\left[2(1-\cos\delta)(I_1+I_2)+4I_{LO}\sin^2\delta\right]\alpha+(I_1-I_2\cos\delta)^2\\ +I_1^2+I_2^2-2I_1I_2\cos\delta+4I_{LO}^2\sin^2\delta=0.\end{aligned}\tag{6}$$

Equation (6) is a quadratic equation in α. The solutions to the above quadratic equation can be easily found to be

$$\alpha=\frac{-v\pm\sqrt{(v^2-4u\,w)}}{2u}\tag{7}$$

where

$$\begin{aligned}u &= 2(1-\cos\delta)\\ v &= -2(1-\cos\delta)(I_1+I_2)-4I_{LO}\sin^2\delta\\ w &= I_1^2+I_2^2-2I_1I_2\cos\delta+4I_{LO}^2\sin^2\delta\\ &= (I_1-I_2\cos\delta)^2+I_2^2\sin^2\delta+4I_{LO}^2\sin^2\delta.\end{aligned}\tag{8}$$

Thus α can be found without an additional photo detector (PD), provided the current of the LO is known and the +/– sign can be decided. The current of the LO can be found during a calibration process. Upon noting that only one of the signs is the correct solution, we shall now determine it. From (1), we calculate

$$I_1+I_2+2I_{LO}\frac{\sin^2\delta}{1-\cos\delta}=2\alpha+2I_{LO}\frac{\sin^2\delta}{1-\cos\delta}+2\sqrt{I_S\ I_{LO}}\ [\cos(\varphi-\delta)]+2\sqrt{I_S\ I_{LO}}\cos\varphi$$

from which we can write

$$\begin{aligned}2\alpha &= I_1+I_2+2I_{LO}\frac{\sin^2\delta}{1-\cos\delta}-2I_{LO}\frac{\sin^2\delta}{1-\cos\delta}-2\sqrt{I_S\ I_{LO}}\ [\cos(\varphi-\delta)+\cos\varphi]\\ &= \frac{-v-4I_{LO}\sin^2\delta-4(1-\cos\delta)\sqrt{I_S\ I_{LO}}\ [\cos(\varphi-\delta)+\cos\varphi]}{u}\\ &= \frac{-v-4\sqrt{I_{LO}}\left[\sqrt{I_{LO}}\sin^2\delta+(1-\cos\delta)\sqrt{I_S}[\cos(\varphi-\delta)+\cos\varphi]\right]}{u}\\ &= \frac{-v-4\sqrt{I_{LO}}\left[\sqrt{I_{LO}}(1-\cos\delta)(1+\cos\delta)+(1-\cos\delta)\sqrt{I_S}[\cos(\varphi-\delta)+\cos\varphi]\right]}{u}\\ &= \frac{-v-4\sqrt{I_{LO}}(1-\cos\delta)\left[\sqrt{I_{LO}}(1+\cos\delta)+\sqrt{I_S}[\cos(\varphi-\delta)+\cos\varphi]\right]}{u}.\end{aligned}\tag{9}$$

In practical applications, since it is often the case that $\sqrt{I_{LO}}(1+\cos\delta) > \sqrt{I_S}[\cos(\varphi-\delta)+\cos\varphi]$, 2 α is, thus, always less than or equal to $-v/u$ in (9). Therefore, minus sign in (7) should be chosen. The equation can now be used in the first step to remove self-beating noise described in Section 2.3.

References

[1] J. Zhang, J. Yu, Z. Jia, and H-C. Chien, "400 G transmission of super-Nyquist-filtered signal based on single-carrier 110-GBaud PDM QPSK with 100-GHz grid," *J. Lightw. Technol.*, vol. 32, no. 19, pp. 3239–3246, Oct. 2014.

[2] Z. Zhang *et al.*, "Coherent transceiver operating at 61-Gbaud/s," *Opt. Exp.*, vol. 23, no. 15, pp. 18 988–18 995, Jul. 2015.

[3] R. Rios-Muller *et al.*, "Spectrally-efficient 400-Gb/s single carrier transport over 7200 km," *J. Lightw. Technol.*, vol. 33, no. 7, pp. 1402–1407, Apr. 2015.

[4] F. Buchali, A. Klekamp, L. Schmalen, and T. Drenski, "Implementation of 64 QAM at 42.66 GBaud using 1.5 samples per symbol DAC and demonstration of up to 300 km fiber transmission," in *Proc. IEEE Opt. Fiber Commun. Conf.*, San Francisco, CA, USA, 2014, pp. 1–3.

[5] T. J. Xia *et al.*, "Transmission of 400 G PM-16 QAM channels over long-haul distance with commercial all-distributed Raman amplification system and aged standard SMF in field," in *Proc. IEEE Opt. Fiber Commun. Conf.*, San Francisco, CA, USA, 2014, pp. 1–3.

[6] G. Raybon *et al.*, "Single-carrier 400 G interface and 10-channel WDM transmission over 4800 km using all-ETDM 107-Gbaud PDM-QPSK," in *Proc. IEEE Opt. Fiber Commun. Conf.*, Anaheim, CA, USA, 2013, pp. 1–4.

[7] S. Chandrasekhar, X. Liu, P. Winzer, J. E. Simsarian, and R. A. Griffin, "Compact all-InP laser-vector-modulator for generation and transmission of 100-Gb/s PDM-QPSK and 200-Gb/s PDM-16 QAM," *J. Lightw. Technol.*, vol. 32, no. 4, pp. 736–742, Feb. 2014.

[8] G. Wang and I. Woods, "Low Vp, high bandwidth, small form factor InP modulator," in *Proc. IEEE Avionics, Fiber-Opt. Photon. Technol. Conf.*, Atlanta, GA, USA, 2014, pp. 41–42.

[9] T. Tatsumi *et al.*, "A compact low-power 224-Gb/s DP-16 QAM modulator module with InP modulator and linear driver ICs," in *Proc. IEEE Opt. Fiber Commun. Conf.*, San Francisco, CA, USA, 2014, p. Tu3H.5, pp. 1–3.

[10] M. Smit *et al.*, "An introduction to InP generic integration technology," *Semicond. Sci. Technol.*, vol. 29, no. 8, pp. 1–42, Jun. 2014.

[11] N. Kikuchi, R. Hirai, and Y. Wakayama, "High-speed optical 64 QAM signal generation using InP-based semiconductor IQ modulator," in *Proc. IEEE Opt. Fiber Commun. Conf.*, San Francisco, CA, USA, 2014, pp. 1–3.

[12] S. J. Savory, "Digital filters for coherent optical receivers," *Opt. Exp.*, vol. 16, no. 2, pp. 804–817, Jan. 2008.

[13] A. Carena, V. Curri, P. Poggiolini, and F. Forghieri, "Dynamic range of single-ended detection receivers for 100 GE coherent PM-QPSK," *IEEE Photon. Technol. Lett.*, vol. 20, no. 15, pp. 1281–1283, Aug. 2008.

[14] Y. Painchaud, M. Poulin, M. Morin, and M. Tetu, "Performance of balanced detection in a coherent receiver," *Opt. Exp.*, vol. 17, no. 5, pp. 3659–3672, Mar. 2009.

[15] Y. Yadin, M. Orenstein, and M. Shtaif, "Balanced versus single-ended detection of DPSK: Degraded advantage due to fiber nonlinearities," *IEEE Photon. Technol. Lett.*, vol. 19, no. 3, pp. 164–166, Feb. 2007.

[16] Y. Feng, H. Wen, H. Zhang, and X. Zheng, "40-Gb/s PolMux-QPSK transmission using low-voltage modulation and single-ended digital coherent detection," *Chin. Opt. Lett.*, vol. 8, no. 10, pp. 976–978, 2010.

[17] X. Zhou, J. Yu, and D. Qian, "A novel DSP algorithm for improving the performance of digital coherent receiver using single-ended photo detection," in Proc. IEEE ECOC, Brussels, Belgium, Sep. 2008, pp. 1–2.

[18] Y.-K. Huang *et al.*, "Filterless reception of 80 $\times$ 112 Gb/s WDM channels using single-ended photodiodes and digital interference reduction," in Proc. IEEE ECOC, Amsterdam, The Netherlands, Sep. 2012, pp. 1–3.

[19] C. Xie *et al.*, "Colorless coherent receiver using 3 $\times$ 3 coupler hybrids and single-ended detection," *Opt. Exp.*, vol. 20, no. 2, pp. 1164–1171, 2012.

[20] D. Rafique, "Fiber nonlinearity compensation: commercial applications and complexity analysis," *J. Lightw. Technol.*, vol. 34, no. 2, pp. 544–553, Jan. 2016.

[21] M. Sowailem *et al.*, "400 G single carrier 500 km transmission with an InP dual polarization modulator," *IEEE Photon. Technol. Lett.*, vol. 28, no. 11, pp. 1213–1216, Jun. 2016.

[22] Z. Malacara and M. Servin, *Interferogram Analysis for Optical Testing*. 2nd ed. CRC: Boca Raton, FL, USA, 2010.

[23] T. M. Hoang, M. Morsy-Osman, M. Chagnon, Q. Zhuge, D. Patel, and D. Plant, "Phase diversity method for optical coherent receiver," in *Proc. IEEE CLEO*, San Jose, CA, USA, 2015, pp. 1–2.

[24] T. M. Hoang *et al.*, "Phase-diversity method using phase-shifting interference algorithms for digital coherent receivers," *Opt. Commun.*, vol. 356, pp. 269–277, 2015.

[25] X. F. Meng *et al.*, "Two-step phase-shifting interferometry and its application in image encryption," *Opt. Lett.*, vol. 31, no. 10, pp. 1414–1416, 2006.